TEMPORAL AND SPATIAL FLUCTUATIONS OF VELOCITY AND HEAT TRANSFER IN WALL TURBULENCE USING DYNAMIC PIV AND IRT

Shunsuke Yamada
Department of Mechanical Engineering
National Defense Academy
Hashirimizu, 1-10-20, Yokosuka, Kanagawa, 239-8686, Japan
yamadas@nda.ac.jp

Hajime Nakamura
Department of Mechanical Engineering
National Defense Academy
Hashirimizu, 1-10-20, Yokosuka, Kanagawa, 239-8686, Japan
nhajime@nda.ac.jp

ABSTRACT

In this study, the temporal and spatial relationship between the heat transfer and flow fluctuations in wall turbulence is presented. We established the simultaneous measurement system of the flow and temperature distributions with high temporal and spatial resolutions by using a dynamic two-dimension and two-component (2D-2C) PIV and a high-speed infrared thermography (IRT). Using this system, the unsteady flow fluctuation in the *xy* cross section and heat transfer on the heated wall were investigated at Re_τ = 930 in the wall turbulence. In order to discuss the correspondence of the near wall flow and the heat transfer, the characteristic of the velocity and heat transfer were detected from the time history of velocity and heat transfer data by using VITA (Variable Interval Time Averaging) method. The temporal and spatial distributions of velocity and heat transfer calculated from ensemble averaging were investigated.

INTRODUCTION

Recently, the suppression of CO_2 emissions due to global warming and the effective utilization of energy resources such as fossil fuels and natural gas have become important issues. At present, the thermal engine, which is widely used, transduces thermal energy into power and electric energy through the working fluid. The design of a thermal engine with high driving efficiency requires the three-dimensional and unsteady characteristic to be considered because the working fluid in this engine exhibits a turbulent flow.

There are numerous techniques for measuring the forced convective heat transfer in a turbulent flow. The coherent structures, which are induced by ejections and sweeps associated with the bursting phenomenon, are observed near wall region. These coherent motions are important role in the thermal transport process with respect to the convective heat transfer. In order to clarify this transport phenomenon, it is necessary to measure the velocity and convective heat transfer. Iritani et al. (1983) and Ochoa et al. (2005) measured the unsteady temperature on the surface of a heating wall in turbulent heat transfer using a temperature-sensitive liquid crystal. However, the lateral conduction and the thermal inertia on the heating surface were not considered. Pietri et al. (2000) and Tagawa et al. (2001) conducted simultaneous measurement of the temperature and velocity fluctuation using Laser Doppler velocimetry (LDV), cold-wire and hot-wire probes. These sensors had the fast temporal response, but require simultaneous multi-point measurements of the temperature and velocity to clarify the spatial distribution induced by the bursting phenomenon. Therefore simultaneous measurements with the high temporal and spatial resolutions are very difficult, and numerous studies are the direct numerical simulations of the turbulent heat transfer.

Recently, the accuracy of the temperature measurement has been improved by infrared thermography (IRT), and high-speed infrared thermography, which provides high temporal-spatial resolutions, has been developed. For the unsteady measurement of the temporal-spatial convective heat transfer, Nakamura and Yamada (2013) measured the instantaneous and local heat transfer coefficient on the surface of electrically heated thin titanium foil in a turbulent flow and reported the temporal and spatial characteristics quantitatively. In the velocity measurements, since the measurement techniques of PIV/PTV have been improved, the turbulent structure near the wall could be more detail analyzed (Schneiders et al., 2016, 2017). Yamada and Nakamura (2016) also established the simultaneous measurement combined system, by which it is possible to measure the temporal and spatial fluctuations of the velocity and the convective heat transfer, respectively. The corresponding to the velocity and the heat transfer oscillations were clarified.

In this study, we focus on the heat transfer mechanism, of which the coherent motions are induced by the ejection and sweeps associated with the bursting phenomenon. The variable interval time average (VITA) method was suggested for this coherent motion (Blackwelder and Kaplan, 1976). Nagano and Tagawa (1995) performed the trajectory analysis of VITA in the wall turbulence and investigated the relationship between the coherent motions and heat transfer. In present paper, simultaneous measurement system using a dynamic two-dimension and two-component (2D2C) PIV and a high-speed

and high-sensitivity IRT with high spatial resolution was constructed. In wall turbulence, the steamwise velocity fluctuation in the vicinity of wall was defined as the detection criterion, and the ensemble averaging of the velocity and heat transfer was conducted by VITA. As these results, the temporal and spatial relationship between the velocity and heat transfer were clarified.

EXPERIMENTAL SETUP

The experiments were carried out in an open-type wind tunnel having a rectangular cross section of 400 mm in height and 150 mm in width, *w*, as shown in Fig. 1(a). The working fluid was air. A flat plate (aluminium and heated plate) of 1200 mm in length was placed horizontally at mid-height in the wind tunnel. A test plate, the wall of which was heated for heat transfer measurement, was positioned behind the aluminium plate across a thermal insulator (balsa wood having a streamwise length of 1 mm) without a vertical step. The origin of the coordinate system used in the present study was located at mid-span of test plate at the heating start point. In this coordinate system, *x*, *y* and *z* denote the streamwise, transverse and spsnwise directions. The streamwise turbulent intensity of the mainstream was approximately 0.5 %. The mainstream velocity, u_0 was set at 4 m/s. The Reynolds number, Re_τ based on the channel half width, δ, and the skin friction velocity upstream of the heating start point was set at 930.

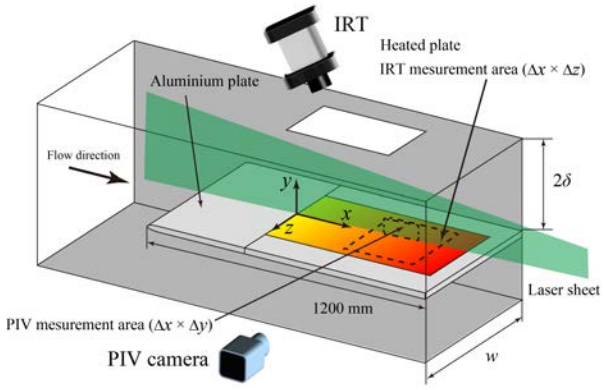

(a) Wind tunnel

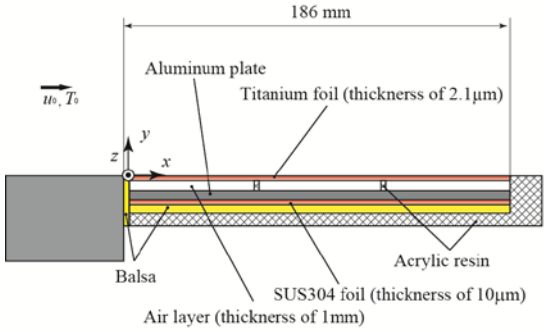

(b) Heated plate

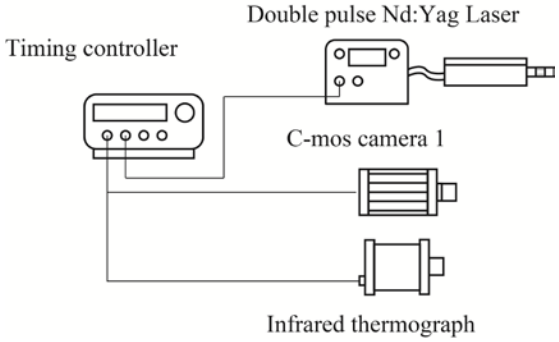

(c) Simultaneous measurement system

Figure 1. Schematic diagram of the experimental apparatus

Fig. 1(b) shows a schematic diagram of the heated plate. The heated plate was fabricated from acrylic resin and had three sections removed. These sections were covered with thin titanium foil sheets (61 mm in length, 100 mm in width, and 2.1 μm in thickness) arranged in the streamwise direction. In the heated plate, air layers, δ_a, 1 mm in thickness exist between the heated titanium foil and the aluminium plate (see Fig. 1(b)). Since the titanium foil and the aluminium plate were heated to approximately the same temperature, the heat conduction loss inside the titanium foil sheets was suppressed. The temperature inside the heated aluminium plate was measured by thermocouples (TC) at x = 63 and 124 mm. Both sides of these thin foils were tightly adhered to electrodes with a high-conductivity bond in order to suppress contact resistance. The three sheets of these foils were heated by direct current so that the temperature difference between the surface of this foil and the mainstream flow was approximately 20 °C. The titanium foil sheets were stretched in response to tension, because the thermal expansion coefficient of the heated acrylic resin is greater than that of the titanium foil. The RMS (root-mean-square) value of the vertical displacement of the thin foil against the fluctuating flow measured using a laser displacement meter was approximately 2 μm. The surface of the thin foil was measured using IRT, so that high-speed thermal fluctuation was observed due to the low heat capacity of the thin titanium foil.

SIMULTANEOUS MEASUREMNET USING PIV AND IRT

In terms of the simultaneous measurements of heat transfer and velocity, the shutter of C-mos camera (Motion Scope M3, IDT, Inc.) and IRT(SC4000, FLIR systems, Inc.), and the emission of a double-pulse laser (HFYA-10SD, Seika Digital Image corp.) were synchronized by a timing controller (LC880-DU1, LabSmith) in Fig. 1(c). The shutter of these cameras and IRT were controlled by this controller for the simultaneous sampling of two-component velocities and temperature. The laser light sheet was located at z = 0 in *xy* cross section. The dynamic 2D2C PIV and IRT frame rate for velocity and temperature measurement was set at 1000 frames per second (fps). PIV and IRT measurement area were $\Delta x \approx \Delta y \approx 10$ mm and $\Delta x \approx \Delta z \approx 60$ mm in Fig. 1(a). In order to confirm accuracy of the velocity measured by this PIV, the temporal-averaging and RMS values of the streamwise and transverse velocities were compared with the DNS data (Abe et al. 2004) in Figs. 2 at $Re_\tau = 350, 920$. To calculate the skin friction velocity, the Clauser chart method was used for a logarithmic low of the mean streamwise velocity (Fernholz and Finley, 1996). The profiles in the present study are coincident with the results of DNS from the viscous sublayer to logarithmic layer in Fig. 2(a). As shown in Fig. 2(b), both the

present study and DNS data are agreement and the transverse position with this RMS peak value are considered to be consistent. The RMS profile of the transverse velocity in the present study is slight difference from the DNS data in a viscous sublayer in Fig. 2(c), however, is generally coincident in a logarithmic low.

CALCULATION PROCEDURE OF CONVECTIVE HEAT TRANSFER

The temperature distributions, T_w on the surface of the titanium foil photographed by IRT was obtained from the following equation:

$$E = \varepsilon\, f(T_w) \;+\; (1-\varepsilon)\, f(T_{amb}) \qquad (1)$$

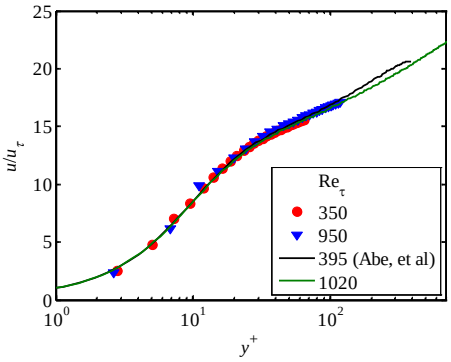

(a) Time-averaging of sramwise velocity

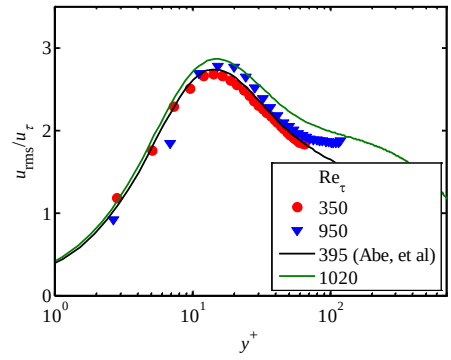

(b) RMS of sramwise velocity

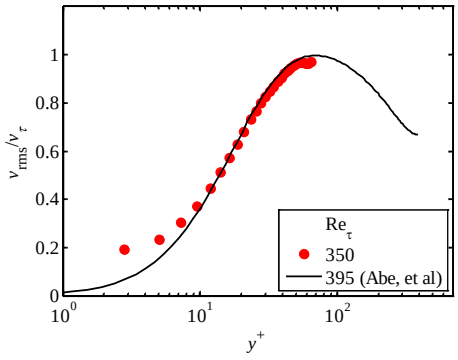

(c) RMS of transverse velocity

Figure 2. Compasrion of velcity data using PIV and DNS

where E is the spectral emissive power detected by IRT, $f(T)$ is the calibration function of the IRT, and ε is the spectral emissivity of the foil for IRT. The terms on the right-hand side of Eq. (1) denote the emissive power from the test surface, T_w, and the ambience, T_{amb}, respectively. In this measurement, the distance between IRT and the test surface was approximately 400 mm, so that the transmittance of the air was approximately 1.0.

Fig. 3 shows a schematic diagram of the heat transfer model from the heated plate. The local and instantaneous heat transfer coefficients were obtained from the following equations:

$$h = \frac{\dot{q}_{in} - \dot{q}_{cd} - \dot{q}_{rd} - \dot{q}_{rdi} + A - B}{T_W - T_0} \qquad (2)$$

where

$$A = \lambda_t \delta_t \left(\frac{\partial^2 T_W}{\partial x^2} + \frac{\partial^2 T_W}{\partial z^2} \right) \qquad (3)$$

and

$$B = c_t \rho_t \delta_t \frac{\partial T_W}{\partial t} \qquad (4)$$

where c_t, ρ_t, λ_t and δ_t are specific heat, density, thermal conductivity and the thickness of the titanium foil, respectively. And $\dot{q}_{in}$ is the input heat fluxes to the foils due to the Joule heating, $\dot{q}_{cd}$ is the heat flux from the foil due to the conduction, and $\dot{q}_{rd}$ and $\dot{q}_{rdi}$ are the radiation heat fluxes away from and into the heated plate, respectively The inverse heat conduction equation, given by Eq. (2), includes both lateral heat conduction though the foil given by Eq. (3) and the temporal delay due to the heat capacity of the foil given by Eq. (4). The heat conduction to the air layer inside the heated plate was calculated based on the temperature distribution inside the air layer (thickness δ_a = 1 mm in Fig. 3), which can be determined by solving the following heat conduction equation:

$$\dot{q}_{cd} = -\lambda_a \left(\frac{\partial T_a}{\partial y} \right)_{y=0} \qquad (5)$$

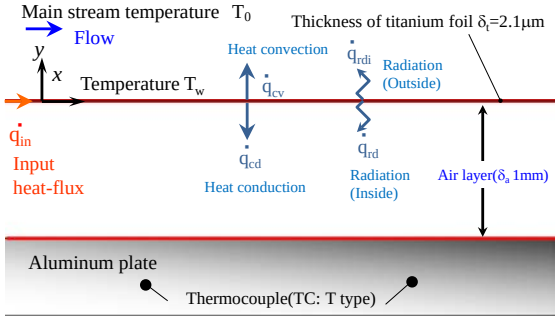

Figure 3. Restroing model of heat transfer ceofficinet

and

$$c_a \rho_a \frac{\partial T_a}{\partial t} = \lambda_a \left(\frac{\partial^2 T_a}{\partial x^2} + \frac{\partial^2 T_a}{\partial y^2} + \frac{\partial^2 T_a}{\partial z^2} \right) \qquad (6)$$

where c_a, ρ_a and λ_a are specific heat, density and thermal conductivity of the air. Since the temperature of the aluminium plate inside the heated plate was assumed to be steady and uniform, the boundary condition on the aluminium plate side can be assumed to be the mean temperature of the aluminium plate as measured by the calibrated thermocouples (TC). The temperature of the air layer inside the heated plate given by Eq. (6), T_a, was calculated using the alternative direction implicit (ADI) method with respect to the x and z directions.

The finite difference method was used to calculate the heat transfer coefficient, h, using Eq. (2). The spatial derivative terms of Eq. (3) were calculated using the second-order central difference with the pixel spacing ($\Delta x \approx \Delta z \approx 0.53$ mm). Moreover, the temporal derivative term of Eq. (4) was calculated using the central difference with the time step of a frame interval (the flame rate of IRT is 1000fps; $\Delta t = 1/1000$ second). A low-pass filter was applied to the temporal and spatial directions (cut-off frequency $f_{cut} < 100$ Hz, the cut-off wavenumber $k_{cut} < 0.33$ mm^{-1}), respectively (Nakamura and Yamada, 2013).

EXPERIMENTAL RESULTS AND DISCUSSIONS

Instantaneous velocity and heat transfer profiles

Figures 4-6 show the instantaneous distributions of the streamwise and transvers velocities at $z^+ = 0$ and heat transfer coefficient on the heated plate, respectively. Also, time history of these distributions represent from (a) to (c) for 2 ms. When the

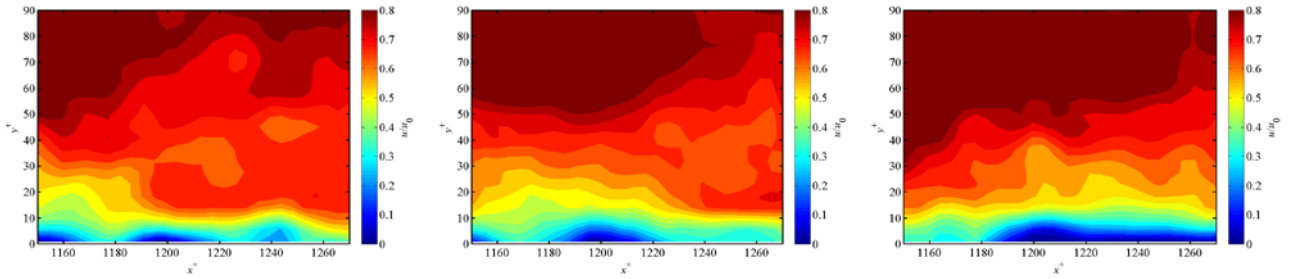

(a) t = 0ms (b) t = 1ms (c) t = 2ms

Figures 4 Time history of streamwise velocity

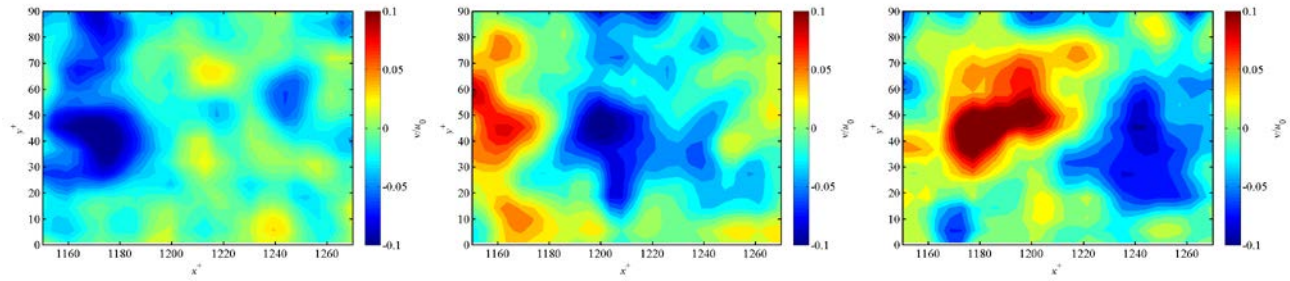

(a) t = 0ms (b) t = 1ms (c) t = 2ms

Figures 5 Time history of transverse velocity

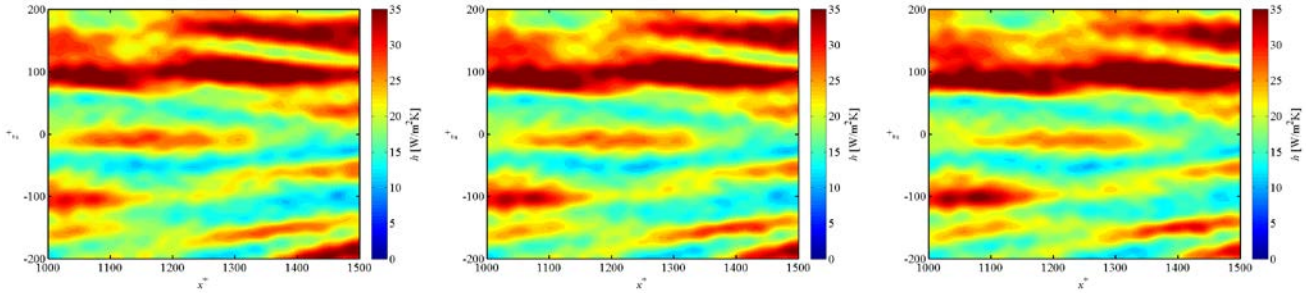

(a) t = 0ms (b) t = 1ms (c) t = 2ms

Figures 6 Time history of heat transfer coefficient

decreasing region of the streamwise velocity appear at (x^+, y^+) ≈ (1180, 30) in Fig. 4(a), the downwash flow of the transverse velocity corresponds to this region in Fig. 5(a). And this decreasing region and the downwash flow convect in the streamwise direction in Figs. 4(a)-(c) and 5(a)-(c). Fig. 6(a) shows that the thermal streaks appear as the increasing of the heat transfer and these streaks expand in the streamwise direction. Also, this maximum of the heat transfer has the periodic structure in spawise direction. The peak of the heat transfer appears in the x^+ region of 1100 to 1300 at z^+ = 0, and convects in the streamwise direction in Figs. 6(a)-(c),

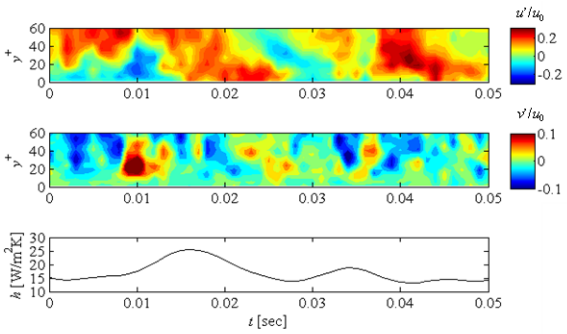

Figure 7. Temporal flucatuation of veloctiy and heat transfer coefficiente at (x^+, z^+) = (1210, 0)

Figure 7 show the temporal fluctuations of these velocities difference from the mean velocities, u', v' and the heat transfer coefficient at (x^+, z^+) = (1210, 0), respectively. In Fig. 7, the decreasing of the streamwise velocity and upwash flow are observed at t = 0.01 s. As a passage of time, the flow accelerates in the seamwise velocity, and the downwash flow appears in the y^+ ≈ 20 at t = 0.015 s. The position of this flow corresponds to that of the high heat transfer coefficients.

Ensemble-averaged velocity and heat transfer

To detect the relationship between the fluctuations of the velocity and the heat transfer, the ensemble-averaged velocity fluctuations, u', v', were detected by VITA method. The busting events changing from "ejection" to "sweep" are observed in the wall turbulence using this method. Initially, the localized variance of the streamwise velocity, var(t), was defined by Eq. (7)

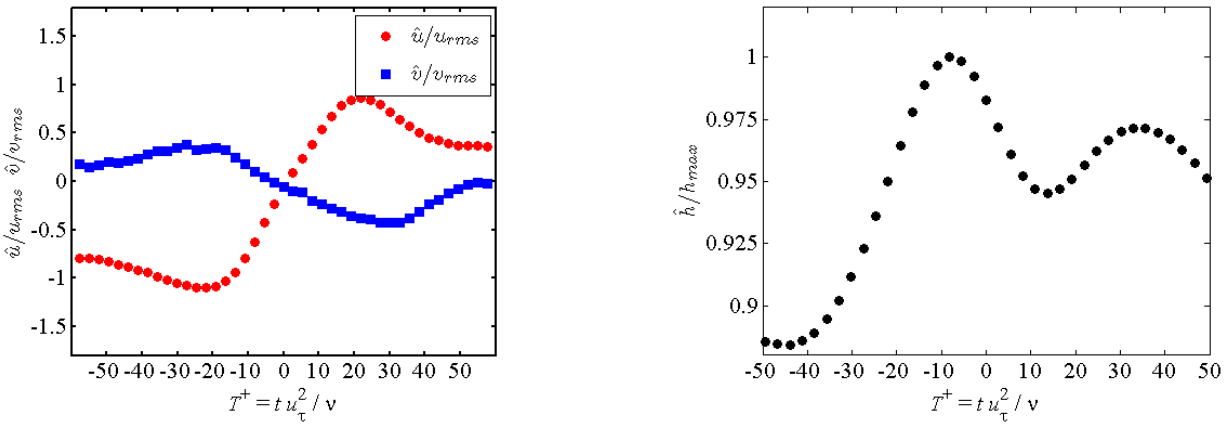

(a) Streamwise and transverse velocities at y^+ = 14.1

(b) Heat transfer coefficient

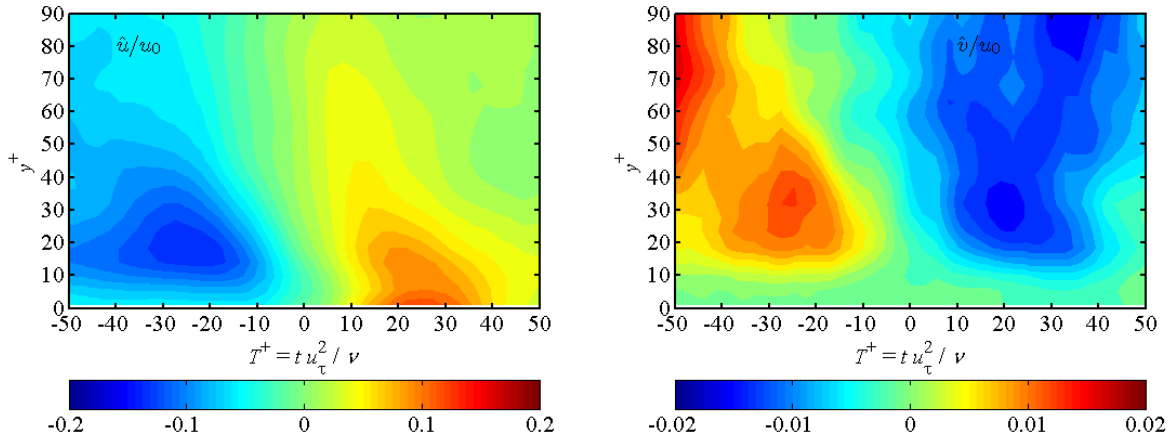

(c) Temporal-spatial distribution of streamwise velocity

(d) Temporal-spatial distribution of transverse velocity

Figure 8. Ensemble-averaging velocity and heat transfer at mid-span

$$\mathrm{var}(t) = \frac{1}{t_1}\int_{t-t_1/2}^{t+t_1/2} u'^2(s)ds - \left[\frac{1}{t_1}\int_{t-t_1/2}^{t+t_1/2} u'(s)ds\right]^2 \quad (7)$$

where t_1 which, is the averaging time, determined, $t_1 \times u_\tau / \nu$ = 27.4, in this study. The variance signal of the velocity at y^+ = 14.1 was calculated. Then, the characteristic velocity profile was detected by Eq. (8)

$$D(t) = \begin{cases} 1 & if \quad \mathrm{var}(t) \geq k\, u_{rms}^2 \\ 0 & otherwise \end{cases} \quad (8)$$

where $D(t)$, k and u_{rms} are the detection function, the threshold level and the root mean square of the total of the streamwise data. The threshold parameter, k, was set at 1.0, when the detection number was the largest. The ensemble-averaging of the streamwise and transverse velocity, and the heat transfer coefficient based on time, $D(t)$ = 1, for $-50 < T^+ (= t \times u_\tau^2 / \nu) < 50$ was conducted.

Figures 8(a)-(d) represent the ensemble-averaged streamwise and transverse velocity profiles, $\hat{u}$ and $\hat{v}$, in the xy cross section, and heat transfer coefficient, $\hat{h}$, on the heated wall. The horizontal axis is non-dimensional time, T^+. As shown in Fig. 8(a) and 8(b), the decreasing of the streamwise and the upwash flow corresponds to the low heat transfer region in $-50 < T^+ < -20$. When the streamwise and the transverse velocities have the inflection points, the maximum of the heat transfer appear around $T^+ = 0$. Also, the high heat transfer region occurs in $20 < T^+ < 50$, due to the acceleration of streamwise velocity and the increasing of downwash flow.

As shown in Fig. 8(c), the minimum of the steamwise velocity appears at $(x^+, y^+) \approx (-20, 20)$. Adversely, the maximum of the velocity approaches near wall region at $x^+ \approx 25$. Fig. 8(d) shows that the peak value of the upwash and downwash flow are observed at $y^+ = 30$. The strong accelerations of the streamwise velocity and the downwash flow occur in y^+ region of 15 to 20 for $-40 < T^+ < -10$. This might mean that there are "ejection" and "sweep" events associated with the bursting events. The accelerations of these velocities decrease at the higher value of y^+. It is for this reason that these velocity phase is more random than below $y^+ = 30$ (Blackwelder and Kaplan, 1976). The enhancement of the heat transfer corresponds to the inflection points of these velocities and the appearance region of "sweep" event.

SUMMARY

We established a simultaneous measurement system that combines Dynamic 2D2C PIV and high-speed IRT in order to investigate the flow and thermal fluctuations in the wall turbulence near the wall. The fluctuation of three velocity components and heat transfer coefficients were simultaneously measured at Re_τ = 930. The characteristics fluctuations of the flow and heat transfer appear in the time history data of these velocity and heat transfer. The ensemble average of these velocities and heat transfer were conducted by VITA method. As these results, the enhancement of the heat transfer corresponds to the inflection points of these velocities and the appearance region of "sweep" event associated with the busting phenomenon.

REFERENCES

Abe, H., Kawamura, H and Matsuo, Y., 2004, "Surface heat-flux fluctuations ina turbulent channel flow up to Reτ = 1020 with Pr = 0.025, 0.71," *Int. J. Heat and Fluid Flow*, 25, pp. 404-419.

Blackwelder, R. F. & Kaplan, R. E., 1976, "On the wall structure of the turbulent boundary layer," *J. Fluid Mech.* 76, pp. 83-112.

Fernholz, H. H., & Finleyt, P. J., 1996, "The incompressible zero-pressure-gradient turbulent boundary layer: An assessment of the data", *Progress in Aerospace Sciences*, 32, 4, pp. 245-311.

Iritani, Y., Kasagi, N.,Hirata, M., 1983, "Heat transfer mechanism and associated turbulent structure in the near-wall region of a turbulent boundary layer," *4th symposium on Turbulent Shear Flow*, pp. 223-234.

Nakamura, H. and Yamada, S., 2013, "Quantitative evaluation of spatio-temporal heat transfer to a turbulent air flow using a heated thin-foil," *Int. J. Heat and Mas Transfer*, 64, pp. 892-902.

Nagano, Y., and Tagawa, M., 1995, "Coherent motions and heat transfer in a wall turbulent shear flow", *J. Fluid Mech.* 305, pp. 127-157.

Ochoa, A. D., Baouhn, J. W. and Byerley, A., 2005, "A new technique for dynamics hear transfer measurements and flow visualization using crystal thermography," *Int. J. Heat and Fluid Flow*, 26, pp. 264-275.

Pietri, L., Aielh, M. and Anselmet, F., 2000, "Simultaneous measurements of temperature and velocity fluctuations in a slightly heated jet combined wire and Laser Doppler Anemometry," *Int. J. Heat and Fluid Flow*, 21, pp. 22-36.

Schneiders, F.G. J, Scarano, F. and Elsinga, G., 2017, "Resolving vorticity and dissipation in a turbulent boundary layer by tomographic PTV and VIS+", *Exp. Fluids*, 58:27, DOI:10.1007/s00348-017-2318-x

Schneiders , J. F. G., Probsting, S., Dwight, R. P., Oudheusden, B. V. W. and Scarno, F., 2016, "Pressure estimation from single-snapshot tomographic PIV in a turbulent boundary layer", *Exp. Fluids*, 57:53, DOI:10.1007/s00348-016-2133-9

Tagawa, M., Nagaya, S. and Ohta, Y. 2001, "Simultaneous measurements of velocity and temperature in high-temperature turbulent flow: a combination of LDV and three-wire temperature probe," *Exp. Fluids*, 30, pp. 143-152.

Yamada, S. & Nakamura, H., 2016, "Construction of 2D-3C PIV and high-speed infrared thermography combined system for simultaneous measurement of flow and thermal fluctuations over a backward facing step", *Int. J. Heat and Mas Transfer*, 61, part A, pp. 174-182.